

# Photomolecular Effect: Visible Light Absorption at Water-Vapor Interface

Yaodong Tu<sup>1</sup>, Gang Chen<sup>1\*</sup>

## Affiliations:

<sup>1</sup>Department of Mechanical Engineering, Massachusetts Institute of Technology, Cambridge, MA 02139.

\*Corresponding author. Email: [gchen2@mit.edu](mailto:gchen2@mit.edu).

**One-Sentence Summary:** Photons in the visible spectrum where bulk water normally does not absorb can cleave off large water clusters from the water-vapor interface.

The evaporation of water is ubiquitous in nature and industrial technologies. The known mechanism for evaporation is “thermal evaporation” which highlights the energy input for evaporation is via heat. Due to the weak absorption of water to visible light <sup>1,2</sup>, the first step to using solar energy to evaporate water is usually by converting it into thermal energy through photothermal processes via additional absorbing materials <sup>3-8</sup>. Contrary to this conventional wisdom, we report here strong absorption of photons in the visible spectrum at the water-vapor interface by direct cleavage of water clusters via a process we call photomolecular effect. We show that this process happens at the water-vapor interface by measuring the dependence of the photomolecular evaporation rate on the wavelength, the angle of incidence, and the polarization of the incident light. The spectra signatures in the vapor phase further support the photomolecular effect. Despite the long propagation lengths of visible light in bulk water, we demonstrate that they can heat a thin layer of fog easily, suggesting that this process is ubiquitous. The photomolecular effect will have significant implications for the earth’s water cycle, global warming, plant transpiration, as well as different technologies involving the evaporation of liquids from drying to power generation.

**Conceptual Picture of Photomolecular Evaporation Process.** The photomolecular effect is a process that happens at liquid-vapor interfaces (Fig.1a), here the water-air interface <sup>9</sup>. This process in some ways mimics the photoelectric effect discovered by Hertz <sup>10</sup> and explained by Einstein <sup>11</sup>, but with major differences in that (1) it happens in the spectrum range where the liquid itself may not necessarily absorb, (2) no electronic transitions are involved, and (3) molecular clusters can be excited and evaporated. There are several ingredients for the “perfect storm” to happen. First, the density of water changes over a distance of a few angstroms ( $\sim 3-7 \text{ \AA}$ ) from the liquid to the vapor phase <sup>12,13</sup>. Second, the incident light creates a huge electrical field gradient over the interfacial region. Based on the macroscopic Maxwell equations, the displacement field of the electromagnetic wave perpendicular to the interface is continuous at the interface, i.e.,  $\epsilon_1 E_{1\perp} = \epsilon_2 E_{2\perp}$ , where  $\epsilon_1=1$  for air and  $\epsilon_2=1.8$  for water in the visible spectrum, and the subscript  $\perp$  emphasizes the direction perpendicular to the interface <sup>14</sup>. This condition means that the electrical field in the perpendicular direction is reduced by nearly a factor of two from air to water over a distance of a few angstroms, creating a large field gradient. Third, water molecules are polar and form instantaneous clusters, although details of the clusters are still under debate <sup>15-19</sup>. The dipole moment of a single water molecular is 1.8D and increases with cluster size <sup>20</sup>, which means an effective charge separation of  $0.5 \text{ \AA}$  or larger. Hence, the electrical field change over the distance of a single water cluster is appreciable. Due to this variation, the force acting on the positive and negative charges of water molecules do not cancel out, leading to a net force, i.e., the quadruple force <sup>14</sup>, acting on the molecular clusters and pulling them from the interfacial region to the adjacent free space. This is similar in some ways to the surface photoelectric effect, which is also due to the large electrical field across  $1-2 \text{ \AA}$  where the electron density changes across the interface <sup>21-23</sup>. From the quantum picture of light, the interaction of a photon and a molecular cluster needs to conserve energy and momentum. Momentum conservation is satisfied because of the rapid change of the electrical field in the perpendicular direction, as is the case for the surface photoelectric effect <sup>22</sup>. For energy conservation, a typical hydrogen bond energy in water is 0.26 eV, which does not match that of a photon at 500 nm with an energy of 2.48 eV. Furthermore, while the bonds within a cluster are dominantly hydrogen bonds, the bonding of a cluster with its environment is usually non-hydrogen-bond, i.e., the van der Waals bond, which is only  $\sim 0.013 \text{ eV}$  (24). Hence, if a 500 nm photon can cleave off a water cluster, it will break at least 10 hydrogen bonds or  $\sim 100$  van der Waals bonds. In Fig.1b, we illustrate the energy conservation of a photon

cleaving off a water cluster, assuming that the average bond energy broken is  $\Delta_1$  and the cluster has  $n$ -bonds with its environment. We emphasize that this does not mean there are  $n$  water molecules in the cluster. We had recently conceived this photomolecular effect in light-driven evaporation from hydrogel samples with large surface areas <sup>9</sup>. In this paper, we report the direct observation of the photomolecular effect from a pure water surface.

**Time History of Water Weight Change Under Light Emitting Diodes (LEDs).** We first demonstrate the photomolecular effect by directly measuring the weight change of water (Methods, Extended Data Fig.1) under the illumination of a green LED with a wavelength of 520 nm. The key to observing the photomolecular effect is the existence of an electrical field in the direction perpendicular to the interface, which means the incident light should not be at normal incidence. Fig.1c shows the time history of the water weight change before and after the light was turned on and off for light incident at 30° from the normal direction, and Fig.1d shows the corresponding evaporation rate as well as the water surface temperature measured in an open laboratory environment (temperature 22.2 °C and relative humidity 26%). During natural evaporation without the LED illumination (AB in Fig.1c), the evaporation rate is constant, and the surface temperature drops below that of the ambient (Fig.1d). When the LED is turned on at point B, we can see that the weight of the water container is reduced quickly. In contrast, no weight change is observed when light from the same LED is incident at 0° (Extended Data Fig.2). No light-driven evaporation at normal incidence is expected because 520 nm light is weakly absorbed and has a penetration depth of ~32 m in pure water <sup>2</sup>, however, the response at 30° is quite surprising indicating that the photomolecular effect is at play. The evaporation rate under light depends on time (Fig.1d), highest at the initial stage, and gradually tapers off until it approaches the natural evaporation rate between BC. The water surface temperature increases during this period (Fig.1d). Between CD, the evaporation rate is the same as that of the natural evaporation and the water surface temperature is also a constant. Even more surprisingly, when light is turned off at point D, the weight of the container increases between DE, suggesting that the evaporated molecules condense back. We found that this weight recovery depends on the ambient conditions (Fig.1c, Methods, Extended Fig.3). When the humidity is above 26%, the weight recovery is complete such that the subsequent natural evaporation (EF) happens along the initial evaporation curve, as the dashed line in Fig.1c shows, as if the light just lifted off the water molecules and put them back to the container when turned off, a phenomenon we call photomolecular levitation. When humidity is at 14%, the weight did not increase after turning off the light (Extended Data Fig.3). Fig.1e shows the weight loss history and evaporation rate when water is first electrically heated to a temperature of 45 °C. In this case, the higher evaporation rate after the light is turned on can be maintained, and no weight recovery can be observed after the light is turned off. Also in this case, immediately when the light is turned on, the liquid surface temperature first decreases and then increases, saturating at ~0.8 °C above that of the surface temperature under natural evaporation (Extended Data Fig.4).

The above light-induced evaporation phenomena can be understood based on the photomolecular effect. When light is at off-normal angles of incidence, the normal component of the electric field is non-zero, leading to a quadrupole force exciting water clusters out of the interface. We will show later that these clusters are much heavier than air molecules. Since the water surface temperature is lower than the ambient temperature when the container is not electrically heated, natural convection does not happen and the cluster transport is purely by diffusion. Some clusters will collide with air molecules and break up into smaller clusters and individual molecules until the air in the local region reaches the maximum humidity. As more

clusters are cleaved off, they accumulate near the surface region and form a cluster layer, with decreasing cluster size away from the interface due to the cluster dissociation. The newly excited water clusters will collide with these accumulated clusters and be reflected into the liquid, generating heat in this recondensation process. This explains why the evaporation rate is highest when light is turned on and then decreases with time, accompanied by the water temperature increases between the BC period in Figs.1c and 1d. At the steady state (between CD period), the net rate of cluster generation between those leaving the surface and recondensed back is equal to the natural evaporation rate of the individual molecules' diffusion to the ambient air. These individual molecules could be directly evaporated from the water surface by either thermal evaporation or cluster dissociation. We call the recondensation of molecular clusters the internal photomolecular effect because recondensation generates heat, with the steady state temperature rise determined by the energy balance of this heat generation to the evaporative cooling and natural convection with the environment (Methods). In comparison, in the absence of light, the steady state temperature is determined by the balance of the heat absorbed due to bond breaking when individual molecules are thermally evaporated and heat transfer of water with the ambient (Methods). When light is turned off, clusters hovering above the water surface condense back, further increasing water temperature (Fig.1d). At lower humidity (Extended Data Fig.3), the mass diffusion flux to the ambient is larger than cluster recondensation after the light is turned off. However, some recondensation still happens, which explains why the evaporation rate after light-off could be even smaller than that of natural evaporation (Extended Data Fig.3). When the water is heated electrically, it creates a rising plume above the surface, which can carry some of the excited clusters away from the water surface, sustaining a continuous high evaporation rate under light, as we observed in the experiment (Fig.1e). In this case, when light is turned on, the water surface temperature has an observable decrease first, followed by an increase until it approaches a constant. The initial decrease is likely due to the heat absorption when clusters break bonds with surrounding water molecules. When molecular clusters can leave the surface, we call it the external photomolecular effect.

**Weight Loss Sensitivity to Light Polarization.** The above mechanism behind the photomolecular effect suggests that we should see different evaporation rates under different polarization of the incident light. We use a green laser diode (532 nm) with linearly polarized output to show the effect of the light polarization (Methods, Extended Data Fig.1e). The weight loss histories under the transverse magnetic (TM wave) and the transverse electric (TE) radiation at 30° angle of incidence are shown Fig. 1e. When the electrical field is polarized in the plane of incidence (TM wave) such that an electric field component normal to the interface exists, we see an increase in the evaporation rate. However, when the electrical field is parallel to the interface (TE wave), the evaporation rate is identical to that of natural evaporation. This light polarization-dependent evaporation rate is consistent with the photomolecular mechanism presented in Fig.1a.

**Photomolecular Evaporation Rate Dependence on Wavelength, Angle of Incidence, Intensity, and Temperature.** We define the difference of the initial evaporation rate from that of the natural evaporation rate as the photomolecular evaporation rate (photomolecular rate for short) as marked in Fig.1d. We mainly focus on discussing the initial evaporation rate under light excitation because it best reflects the photomolecular effect, although keep in mind that even this rate depends on the environmental conditions as we noted before. Figs.2a-2f show the dependence of the photomolecular rate on the wavelength, the angle of incidence, the intensity, and the temperature, which further support the photomolecular evaporation mechanism.

Fig.2a shows that the photomolecular effect happens only for photons with a wavelength shorter than 650 nm and peaks at 520 nm, although the exact starting wavelength and the peak positions are unclear due to the discrete nature of our light sources. We had observed the highest evaporation rate at the same wavelength in hydrogel-evaporation experiments<sup>9</sup>. The wavelength-dependent behavior of the photomolecular effect is very similar to that of the photoelectric effect. Only photons with energy larger than the bonding energy of the water clusters with surrounding water molecules can cleave off water clusters (Fig.1b). We interpret that the wavelength corresponding to the peak photomolecular rate occurs when photons at this wavelength best match the cluster's bonding energy with surrounding water molecules. Shorter wavelength photons likely will waste some of their excess energy as cluster's kinetic energy (Fig.1b). We will estimate the size of water clusters later. Interestingly, the peak absorption happens at a wavelength that bulk water is least absorbing.

Fig. 2b plots the photomolecular rate dependence on the angle of incidence for LEDs of different wavelengths, the TM-polarized 532 nm laser radiation, and light from a solar simulator. All light sources are at  $1000 \text{ W/m}^2$ , i.e., equivalent to that of the intensity of standard 1 sun. Both LED and laser diode light sources are divergent, and thus the angle is only nominal (Methods). Also, due to the different beam shapes of the LED and the laser diode, we do not make a direct comparison of the magnitude of the photomolecular rate, which is affected by the diffusion of individual molecules to the ambient and hence is dependent on the container size. We can see from the figure that very little evaporation happens at the normal incidence for all lights because in this case, the electric field of the incident light is parallel to the water surface. A peak of the photomolecular rate exists between  $30^\circ$ - $40^\circ$  for all light sources because the loss in the photon flux at a larger angle of incidence overweighs the increase in the perpendicular electric field.

Figure 2c shows the photomolecular rate dependence on the light intensity. At low intensities, the dependence is linear. As the intensity goes beyond 1 sun, the evaporation rate tends to be slightly sublinear, indicating a saturation trend, which could be due to the slower rate of formations of fluctuating clusters in the interfacial region than the rate of photon influx.

When water is heated and the light is on, thermal evaporation happens concurrently with photomolecular evaporation. In Fig.2d, we show both the photomolecular and thermal evaporation rates as a function of the water temperature. The photomolecular evaporation rate decreases while the thermal evaporation rate increases with increasing temperature, however, the dependences of the photomolecular rate on wavelength and the angle of incidence are similar to no heating case (Fig.2a and Extended Data Fig. 5). The decreasing photomolecular evaporation rate is likely due to the reduced number of water clusters at higher temperatures<sup>19</sup>.

**Vapor phase spectra and temperature distribution.** If water clusters exist above the water surface, we should be able to see signatures in the vapor phase. In Figs. 3a and 3b, we show the transmission spectra measured in the vapor phase at different heights for the 520 nm LED incident at  $30^\circ$ , when water is heated to  $45^\circ \text{C}$  electrically (Methods, Extended Data Fig.6). The transmission over the vapor region with the light on and light off are distinctively different at the spectrum locations where water vapor absorbs. Under green LED, the spectra show fine structures, especially near the fundamental vibrational wavelength of  $2.74 \mu\text{m}$ <sup>1</sup>, and also at other higher harmonics. The more discrete lines from clusters are due to the splitting of the vibrational modes from that of a single water molecule to many molecules in the cluster.

We measure the temperature profile in the vapor phase using an infrared camera with a glass slide suspended above the water surface as a thermal emission source (Methods, Extended Data Fig.7). The temperature profiles measured at different times further confirm the cluster picture, as shown in Figs. 3c for the case when water is heated. We see that when light is turned on, a much steeper temperature drop near the surface region is observed, followed by a region where temperature distribution is flat. The fast temperature drop between 0-10 mm happens because of heat absorption when clusters are further broken up in the air. The flat region exists because air becomes supersaturated. In this region, the clusters break up and recondense. Further away, with more cold air from ambient drafted into the vapor plume, the temperature continues to drop again. Interestingly, the air temperature far from the surface is lower when the light is on than when the light is off, demonstrating the potential of photomolecular effect for air cooling.

The vapor side temperature profile when water is not heated is also measured (Extended Data Fig.8). In this case, because the water surface is coldest, the temperature profile is inverted, and hence no convection happens as we stated before. In this case, we cannot see a large difference in the transmission spectra between natural evaporation and photomolecular evaporation (Extended Data Fig.9). This is probably because the water clusters are too close to the surface due to the lack of a rising plume when compared to electrically heated water. The relatively large probe beam in the UV-VIS measurement prevents us to probe this cluster layer. The picture that the clusters are close to the surface when water is not heated is also consistent with our observation of the photomolecular levitation phenomenon.

We also observed similar behavior, i.e., the rapid temperature drop, the flat temperature region, and the vapor transmission spectral shift, in hydrogel-based light-driven interfacial-evaporation experiments<sup>9</sup>, although the rapid temperature drop region, as well as the flat temperature region, are both shorter, and the observed spectral change is not as dramatic as from pure water surfaces we observe here. These are consistent with our hypothesis that large clusters generated in the internal surface of the hydrogel are difficult to escape the porous structure until they become smaller due to collision breakup of the clusters. Although hydrogel evaporation under light has shown an evaporation rate over 5 kg/m<sup>2</sup>-hr on a flat surface<sup>24,25</sup> and over 7 kg/m<sup>2</sup>-hr on 3D structures<sup>26</sup>, there is more room for a higher evaporation rate based on our study.

**Estimation of Absorptance and Cluster Size.** The divergent nature of the LED makes a direct measurement of the absorptance difficult. We used the measured temperature difference between the ambient and water under natural conditions and the temperature rise of water under light i.e.  $\Delta T$  in Fig.1d, to estimate the absorptance (Methods). This temperature rise is shown in Fig.2e for green and red LEDs. Under green LED, the temperature rise peaks at 30° where the photomolecular rate is highest (Fig.2a), while the red LED shows monotonically decreasing temperature rise with increasing angle, consistent with the bulk absorption behavior. We explained before that  $\Delta T$  is due to the recondensation of water clusters which releases heat. At steady state, i.e., region CD in Fig.1c, the absorptance  $\alpha$  can be estimated from energy balance  $\alpha I A \cos\theta = h_e A_t \Delta T$  (Methods), where  $I$  is the light intensity,  $\theta$  the angle of incidence,  $h_e$  the effective convective heat transfer coefficient between the sample and the ambient at a temperature  $T_\infty$ ,  $A$  the top evaporating surface area and  $A_t$  the total surface area for heat transfer. We estimate  $h_e A_t / A$  based on the natural cooling data (Methods) and use the above relationship to calculate the absorptance. Fig. 2e gives the estimated absorptance as a function of the angle of incidence for

the green LED, which shows an absorptance of  $\sim 7.6\%$  at  $30^\circ$ . Using this absorptance for the 520 nm LED and measured photomolecular evaporation rate of  $1.01 \text{ kg/m}^2\text{-hr}$  for  $1000 \text{ W/m}^2$  incidence, the normalized photomolecular evaporation rate can be  $13.3 \text{ kg/m}^2\text{-hr}$  at one sun. This is 9.2 times the thermal limit at  $1.45 \text{ kg/m}^2\text{-hr}$  by converting  $1000 \text{ W/m}^2$  of photon energy in one hour into the equivalent sensible and latent heat of water, assuming evaporation at  $40^\circ\text{C}$  and an ambient temperature of  $25^\circ\text{C}$ . We hasten to point out that this high photomolecular rate is not the limit, as we have not been able to measure an intrinsic photomolecular rate due to its dependence on environmental conditions.

From the photon flux  $N_p$ , the evaporation rate  $\dot{m}$ , and the absorptance  $\alpha$ , we can also estimate the size of molecular clusters excited per photon. The photon flux absorbed at the surface is  $N_p = \alpha I \cos\theta / (\hbar\omega)$ , where  $\hbar\omega$  is the photon energy with  $\hbar$  the reduced Planck constant and  $\omega$  the angular frequency. The average number of water molecules in a cluster is  $N = N_A \dot{m} / (M N_p)$ , where  $\dot{m}$  is the evaporation rate,  $M$  the molar mass, and  $N_A$  the Avogadro constant. Using experimental data, we find that the cluster size  $N$  is between 50 to 60. Although these clusters are surprisingly large, Chaplin's model of water cluster<sup>18</sup> consists of 280 water molecules. How many bonds are broken depends on the configurations of the cluster. If we assume on average two bonds are broken, then there are  $\sim 100\text{-}120$  bonds broken by one photon, suggesting that most of these bonds are weak van der Waals bonds with energy  $\sim 0.013 \text{ eV}$ <sup>15</sup>.

**Fog Heating by Green Light.** For a flat surface, the photomolecular absorption can be maximized by orienting the light to an optimal angle of incidence. For droplets, there are always electrical field directions of the light that are perpendicular to the interface. The increased surface area, the curvature of the droplets, and the multiple scattering effects will further enhance the photomolecular process. Thus, we expect photomolecular effect will be important for clouds and fogs. To demonstrate this, we designed and fabricated a cloud chamber and generated water droplets into the chamber as shown in Fig. 4a (Methods, Extended Data Fig.10 and Movie 1). We shine LED at 1 sun to the cloud chamber and measured the temperature rise of an empty chamber and that with a cloud inside using an IR camera (Extended Data Fig.10). Figs.4b and 4c show that the chamber itself is not heated up, but visible LEDs heat the cloud significantly, peaking at 520 nm, consistent with the internal photomolecular heating mechanism. Past cloud models assumed that liquid water absorption in the visible range is weak due to the small absorption coefficient of bulk water<sup>27</sup>. This simple demonstration suggests that visible light plays important role in water evaporation and the earth's water cycle.

**Discussion.** The above experiments conclusively demonstrate the photomolecular effect: the cleavage of water molecular clusters by photons, in a spectral region that water is least absorbing. We believe that the qualitative pictures we present in Fig.1a and 1b underlie the mechanisms behind the photomolecular process, but recognize that quantitative description of the process will need more effort, especially considering that there is no consensus on what kind of clusters exist in water<sup>19</sup>. The experimental observations we report here may be useful for understanding clusters in water. Since the photomolecular evaporation rates we measure depend on the ambient conditions, one could ask what the intrinsic photomolecular rate is and what the fundamental limit of the rate is. Our current experiment is limited by the stability of the weighing station under open laboratory conditions and cannot resolve these questions. We hypothesize that the cluster reformation after one is cleaved off will impose a limit, as we already see from the slightly

sublinear photomolecular rate in Fig. 2c and the competition between thermal and photomolecular evaporation.

We have shown in another paper <sup>9</sup> that the photomolecular effect is the reason behind recent reports of solar-driven interfacial evaporation from different porous materials exceeding the thermal evaporation limit <sup>8,24-26</sup>. We believe that the same mechanism could also explain past experimental observation of light desorption of water molecules on solid surfaces <sup>28,29</sup>. Our demonstration of the photomolecular effect in fog suggests that this process is ubiquitous: from clouds to fogs, from ocean to soil surfaces, and in plant transpiration. We are wondering whether the fact that leaves are green, i.e., plants avoid green light, is related to our observation that the photomolecular rate is highest at these wavelengths. After all, biological organisms emerged way after the earth has water and sunlight. We often hear from weather forecasts “after the sun thinned the clouds”. In the past, we naturally think this is caused by thermal evaporation, either due to the rising temperature of the air or due to absorption by water of the infrared radiation in the solar spectrum. We now know that photomolecular process could also be at play for this natural phenomenon. While it is well-known that bulk materials’ absorption mainly happens via electronic and vibrational transitions, our work suggests that interfacial photomolecular evaporation, both internal and external, can lead to photon absorption in water and possibly in other liquids or even solids. Further exploration of the effect can lead to new scientific insights and technologies in desalination, waste-water treatment, drying, and air conditioning.

## **Methods**

### **Materials**

DI water (18.2 M $\Omega$ .cm @ 25°C, produced from a Millipore Direct-Q® 5 UV Water Purification System) is used in all experiments. For all the evaporation rate measurements and the vapor transmission spectrum tests, the water container is made of glass. We have checked using UV-VIS that the materials used for the container do not absorb in the wavelength range 350 nm ~ 1000 nm. For experiments using LEDs, the water container is typically 25 mm in diameter, and the depth 3 mm (containers with 12.5 mm was also tested) (Extended Data Fig.1a). We made sure that water does not fall too much below the mouth of the container. And the fog chamber is made of transparent plastic (75mm\*50mm\*17.5mm, the wall thickness is 2.3mm).

For evaporation rate experiments using a laser diode, a slit-like container is made of glass slides (1mm thick) glued together (Krazy super glue) (Extended Data Fig. 1a).

### **Evaporation rate measurement**

Extended Data Figs. 1a-e give some details of the evaporation rate measurement platform. An electronic balance (And EK610i) situated on a lift platform is used to monitor the weight loss of the sample during experiments. The balance is covered with highly reflective mirror film (3M ESR reflector film). To reduce the noise of the measured weight loss during evaporation, an air shield made of transparent plastic film is placed around the lift platform to reduce the airflow around the sample. We also carefully check the lab environment to make sure the fluctuations in the weight’s signal are no more than 0.01g (balance’s precision).

To avoid any possible heating effect due to the small amount of light absorption by the weighing platform, the sample stage is placed on a support structure made by gluing the glass slides using

clear glue. This minimizes heat transfer between the weighing platform and the water sample holder.

**Testing with LEDs:** LED lamps were purchased from Charon with a rated power of 100 W and different wavelengths: purple 390nm, blue 440nm, green 520nm, yellow 590nm, red 650nm, and IR 815nm. To avoid overheating, LEDs need active cooling. We build a water cooling-based LED light source, which not only prevents LED from overheating, but also eliminates additional infrared radiation heating, and avoids generating additional air movement which is a very common problem for air cooling. To reduce the divergence and to improve the uniformity of the flux intensity, we built a light guide using highly reflective films made of a double layer structure: the outside is made of 1 mm aluminum sheet and the inside is a high reflectance plastic sheet mirror (reflectance higher than 92% tested by Cary 5000 UV-VIS spectrometer) glued onto the inside surface of the aluminum cylinder. The light coming out the end of the light tube is still divergent. We made sure that the light spot size is larger than the container area. Due to this divergence, the angle we reported in the figures should be considered as the nominal angle of incidence, measured between the center of the LED and the water surface normal direction. Also due to this divergence, the intensity changes with distance from the light source. As the angle changes, the intensity intercepted by the water surface can be nonuniform. The intensity we report is measured with a detector placed perpendicular to the incoming light at the location equivalent to the center of the sample surface.

To electrically heat water to higher temperatures, we glue a heater (Thermoelectric module from Marlow industries, Inc. Model No: NL1012T-02AC) to the bottom of the water container. We used a battery as the power source for the heater and place the battery also on the weighing platform since external wires increase the platform vibration (Extended Data Fig.1b and Fig.1c). A potentiostat is used to vary the power input to the heater. The potentiostat is also wrapped in metallic foil to reduce its absorption to light.

**Testing with Laser Diode.** A mounted 532 nm laser diode with a rated power of 1 W was also purchased from Charon. The laser diode came with a collimator lens set. With the collimator, the beam divergence is small but the spot size is also small. Furthermore, the spot shape and the polarization of the light depend on the position of the collimator lens. We took out the collimator. In this case, the laser beam is linearly polarized, as confirmed with a  $\frac{1}{4}$  waveplate. The beam is highly elliptical. Hence, we fabricated rectangular water containers as described in Materials (Extended Data Fig.1a). Measurement of evaporation at the two polarizations is made by rotating the laser itself. The rectangular container is also rotated so that the beam spot is larger than the container size.

Both LEDs and the laser diode are placed on a platform that we can rotate to change the angle of incidence. The distance between the center of the sample surface and the light source is maintained at constant during angle change. For the intensity dependence test, the sample stages and all the setups were kept the same. The intensity is varied by changing the input power to the light source.

**Testing with a solar simulator.** We also tested evaporation using a solar simulator (Sciencetech SS1.4K). A reflective mirror is used to change the angle of incidence.

The light intensity is monitored with a thermopile detector (Newport power meter 2936-R with sensor 818P-001-12) to monitor the input light flux intensity before and after one test to make sure the flux intensity is stable. The spatial non-uniformity of the flux intensity of the solar simulator (Sciencetech SS1.4K) is less than 3% for a light spot with 5 cm in diameter.

Most experiments were performed in the laboratory environment. Although room temperature is nearly constant, the environmental humidity varies. We found that the photomolecular evaporation rate depends on the humidity.

### **Temperature measurements**

We used IR cameras (FLIR ETS320) to measure water surface temperature and vapor phase temperature. To make the IR temperature sensing as accurate as possible, we calibrate the IR camera at 19.2 °C (monitored by a calibrated K-type thermal couple, insert the glass slide sensor into a water bath with steady natural evaporation in a lab open environment), and at 45.5 °C (monitored by a calibrated K-type thermal couple, insert the glass slide sensor into a water bath with steady thermal evaporation in a lab open environment driven by a joule heater), by adjusting its emissivity, reflective temperature, background temperature and the distance between the sample and the lens. The difference at 19.2 °C and 45.5 °C between IR microscope and thermocouple readings are less than 0.2 °C and 0.2 °C, respectively.

For vapor temperature measurement, we used an IR microscope together with thermocouples. To use an IR camera to measure the vapor phase temperature distribution, we use a very thin glass slide (0.1mm in thickness) as a thermal emitter for the IR camera to aim at (Extended Data Fig. 7). The glass slide cannot touch the sample surface, so there is a small distance of ~2 mm, which is added in plotting Fig.3c.

Samples of the obtained IR images of water surfaces are shown in Extended Data Fig. 4 and vapor phase temperature is shown in Extended Data Fig. 7. The line plot of temperature variation along height in Fig. 3c is obtained from averaging the temperature distribution 5 mm around the centerline.

### **Direct transmission spectrum of the vapor phase**

We used Cary 5000 UV-VIS spectrometer to measure the transmission spectrum of the vapor at different heights during light-driven evaporation operation. A special sample stage was made with water-cooled LED so that the sample stage can fit into the sample chamber of the UV-VIS-NIR spectrometer (Extended Data Fig. 6). The probe beam of the spectrometer is limited with an IRIS of the size 1mm (vertical) × 3 mm (horizontal) as shown in Extended Data Fig. 6. The height of the sample can be controlled with the help of a movable stage. Since the probe beam is fixed, this configuration enables us to scan the direct transmittance of the moist air at different heights over the working samples, by lowering the sample. The LEDs are fixed in the UV-VIS sample chamber at a 30° angle of incidence. We made sure to make the sample at different heights can receive the same input energy (1 sun) by adjusting the LED input voltage. During testing, the sample chamber was kept closed to reduce the noise, but vapor can leak out since the sample chamber is not hermetically sealed.

Under LED lamp radiation, the detector of the UV-VIS spectrometer easily gets saturated due to scattered light. To avoid this situation, we put two filters with cut-off wavelengths at 530 nm and 610nm in the front of the detector window as shown in Extended Data Fig. 6 to cut off the lights shorter than these wavelengths.

However, the beam shape coming out of the UV-VIS changes along the path length, although along the sample diameter, the change is small. Due to this change, the beam position should be understood as nominal.

We measured the transmission spectrum in the vapor phase at different heights on the water surface. We first measure the transmission of the ambient air as a reference for normalization. For each height, we measure the transmittance with the light off, followed by turning the light on. Each spectral scan takes about 15 min. After measurement of the light off and on spectra, we open the chamber and readjust the height manually. We also add a small amount of water to keep the water level at a similar level.

### **Fog generation and its visible light absorption test**

The fog generation system is illustrated in Extended Data Fig. 10. Here the fog generator is made of an ultrasonic Atomization Maker (20mm in diameter, 113 kHz, from WHDTS@Amazon). To supply water and prevent the generator to heat up, we build a water cooling kit by using a silicone tube and plastic tube. Finally, the water cooling kit is glued to the backside of the ultrasonic Atomization Maker. The fog size according to the product manual is about 3 micrometers in diameter.

To show the fog can absorb visible light due to the photomolecular effect, we use LEDs lamps with various wavelengths as the light sources and an IR camera (FLIR C5) to monitor the fog chamber's surface temperature. The testing sequence consists of the following steps: (1) leave the dry and empty fog chamber on the test platform for 60 minutes, and then monitor its outside top surface temperature for 20 minutes to make sure it gets thermal equilibrium with the surrounding environment; (2) turn on the LED lamp and shine the fog chamber for 60 minutes, and then monitor the outside top surface temperature of the dry and empty fog chamber for 20 minutes to make sure it gets thermal equilibrium with the surrounding environment. This step measures the absorption of the container; (3) turn off the LED lamp and turn on the fog generator, after 30 minutes when the chamber is filling with fog (Fig.4a), start to monitor the outside top surface temperature of the fog chamber for 20 minutes to make sure it gets thermal equilibrium with the surrounding environment; (4) turn off the fog generator, after 30 minutes when almost all the inside fog condense onto the wall, turn on the LED lamp for 60 minutes, and then monitor the outside top surface temperature of the fog chamber for 20 minutes to make sure it gets thermal equilibrium with the surrounding environment; (5) drain out the condensation inside the fog chamber and turn on the fog generator, after 30 minutes when the chamber is filling with fog (Fig.4a), turn on the LED lamp after 30 minutes start to monitor the outside top surface temperature of the fog chamber for 20 minutes to make sure it gets thermal equilibrium with the surrounding environment. For all the measurements under various LED lamps, we keep the light intensity 1 sun and the same distance between the lamp and the fog chamber.

### **Absorptance Determination from Measured Temperatures**

Figure 1d shows the temperature history of water, from which we can determine the heat transfer rate between the sample and the ambient. At the steady state of the natural evaporation, the rate of heat absorbed by the evaporating water is  $\dot{m}L$ , where  $\dot{m}$  is the evaporation rate and  $L$  is the latent heat. This heat absorption is balanced by the heat transfer from the environment to the container. The energy balance is

$$h_e A_e (T_{w1} - T_\infty) = \dot{m}AL \quad (S1)$$

where  $h_e$  is the effective heat transfer coefficient and  $A_e$  is the effective surface area,  $A$  is the top surface area for evaporation,  $T_{w1}$  is the temperature of water and  $T_\infty$  the temperature of ambient. We use effective  $h_e$  and  $A_e$  because the evaporating surface has a different convective heat transfer coefficient than the side and bottom surfaces of the water container. We will only need  $h_e A_e / A$

as a group to determine the absorptance. We can use the measured  $T_{w1}$  and  $\dot{m}$  to determine  $h_e A_e / A$ .

Under light irradiation, water reaches a new temperature as shown in Fig.1d. According to our experiments, the final evaporation rate is the same as natural evaporation, and hence we can assume that  $h_e A_e / A$  remain the same. The new energy balance determining the new water temperature  $T_{w2}$  is

$$h_e A_e (T_{w2} - T_\infty) = \dot{m} A L + \alpha I A \cos\theta \quad (\text{S2})$$

where  $\alpha$  is the absorptance,  $\theta$  the angle of incidence,  $I$  the incoming light intensity, and  $\cos\theta$  accounts for the projected area of the surface relative to the incoming light. Subtracting Eq.(S1) from (S2), we get

$$h_e A_e \Delta T = \alpha I A \cos\theta \quad (\text{S3})$$

where  $\Delta T = T_{w2} - T_{w1}$  is the temperature rise of water under illumination as shown in Fig.1d. Using the measured  $h_e A_e / A$  based on experimental data between period AB in Fig.1d, and  $\Delta T$  between BC, we determined the absorptance as shown in Fig.2f.

The above derivations assume that water is at a uniform temperature at a steady state. This assumption can be justified from the Biot number, which represents the ratio of thermal resistance inside the liquid to that of the surrounding air,

$$Bi = \frac{ht}{k} \quad (\text{S4})$$

where  $t$  is the water layer thickness  $\sim 3$  mm and  $k=0.6$  W/m-K for water. The heat transfer coefficient we determined is  $\sim 20$  W/m<sup>2</sup>-K, leading to  $Bi \sim 0.03$ , which means that most temperature drop happens between water and ambient. The assumption of uniform water temperature is hence justified.

## References

1. Braun, C. L. & Smirnov, S. N. Why is water blue? *Journal of Chemical Education* **70**, 612–614 (1993).
2. Hale, G. M. & Querry, M. R. Optical constants of water in the 200-nm to 200- $\mu$ m wavelength region. *Applied Optics* **12**, 555–563 (1973).
3. Weinstein, L. A. *et al.* Concentrating Solar Power. *Chemical Reviews* vol. 115 12797–12838 (2015).
4. Otanicar, T. P., Phelan, P. E., Prasher, R. S., Rosengarten, G. & Taylor, R. A. Nanofluid-based direct absorption solar collector. *Journal of Renewable and Sustainable Energy* **2**, 033102 (2010).
5. Neumann, O. *et al.* Solar vapor generation enabled by nanoparticles. *ACS Nano* **7**, 42–49 (2012).

6. Ghasemi, H. *et al.* Solar steam generation by heat localization. *Nature Communications* **5**, 1–7 (2014).
7. Wang, Z. *et al.* Bio-inspired evaporation through plasmonic film of nanoparticles at the air–water interface. *Small* **10**, 3234–3239 (2014).
8. Zhao, F. *et al.* Highly efficient solar vapour generation via hierarchically nanostructured gels. *Nature Nanotechnology* **13**, 489–495 (2018).
9. Tu, Y. *et al.* *Photomolecular Effect Leading to Water Evaporation Exceeding Thermal Limit*. arXiv preprint arXiv:2201.10385 (2022).
10. Hertz, H. On an effect of ultraviolet light upon the electric discharge. *Ann. Physik* **31**, 983 (1887).
11. Einstein, A. On a heuristic point of view concerning the production and transformation of light. *Annalen der Physik* **17**, 132–148 (1905).
12. Alejandre, J., Tildesley, D. J. & Chapela, G. A. Molecular dynamics simulation of the orthobaric densities and surface tension of water. *The Journal of Chemical Physics* **102**, 4574 (1998).
13. Dang, L. X. & Chang, T.-M. Molecular dynamics study of water clusters, liquid, and liquid–vapor interface of water with many-body potentials. *The Journal of Chemical Physics* **106**, 8149 (1998).
14. Jackson, J. D. *Classical Electrodynamics*. (Wiley, 1998).
15. Stillinger, F. H. Water revisited. *Science* **209**, 451–457 (1980).
16. Benson, S. W. & Siebert, E. D. A simple two-structure model for liquid water. *Journal of the American Chemical Society* **114**, 4269–4276 (2002).
17. Weinhold, F. Quantum cluster equilibrium theory of liquids: General theory and computer implementation. *The Journal of Chemical Physics* **109**, 367 (1998).
18. Chaplin, M. F. A proposal for the structuring of water. *Biophysical Chemistry* **83**, 211–221 (2000).
19. Ludwig, R. Water: From clusters to the bulk. *Angewandte Chemie International Edition* **40**, 1808–1827 (2001).
20. Gregory, J. K., Clary, D. C., Liu, K., Brown, M. G. & Saykally, R. J. The water dipole moment in water clusters. *Science* **275**, 814–817 (1997).
21. Hüfner, Stefan. *Photoelectron Spectroscopy : Principles and Applications*. (Springer Berlin Heidelberg, 2003).
22. Feibelman, P. J. Surface electromagnetic fields. *Progress in Surface Science* **12**, 287–407 (1982).
23. Liebsch, Ansgar. *Electronic Excitations at Metal Surfaces*. (Springer US, 1997).
24. Guo, Y. *et al.* Tailoring surface wetting states for ultrafast solar-driven water evaporation. *Energy & Environmental Science* **13**, 2087–2095 (2020).
25. Zhang, X., Peng, Y., Shi, L. & Ran, R. Highly efficient solar evaporator based on a hydrophobic association hydrogel. *ACS Sustainable Chemistry & Engineering* **8**, 18114–18125 (2020).
26. Gao, T., Wu, X., Wang, Y., Owens, G. & Xu, H. A hollow and compressible 3D photothermal evaporator for highly efficient solar steam generation without energy loss. *Solar RRL* **5**, 2100053 (2021).
27. Stephens, G. L. Radiation profiles in extended water clouds, I. Theory. *Journal of Atmospheric Sciences* **35**, 2111–2122 (1978).
28. Kawasaki, T., Mochida, T., Katada, J.-I. & Okahata, Y. *Laser Response of a Quartz Crystal Microbalance: Frequency Changes Induced by Light Irradiation in the Air Phase*. *ANALYTICAL SCIENCES* vol. 25 (2009).

29. Sommer, A. P. *et al.* Breathing volume into interfacial water with laser light. *Journal of Physical Chemistry Letters* **2**, 562–565 (2011).

**Acknowledgments:** We would like to thank Dr. Qichen Song for his help in optics and discussion. We also thank Qian Xu and James Zhang for proofreading. G.C. grateful thank MIT for its support and Tracy Chen for listening to his science and mentioning “when the sun thins the cloud”.

**Author contributions:** YDT did all experiments, GC conceived the physical picture and suggested experimental directions, led interpretation of results, and manuscript writing.

**Competing interests:** Authors declare that they have no competing interests.

**Data and materials availability:** All data are available in the main text or supplementary materials.

Extended Figs. 1 to 10

Movies 1

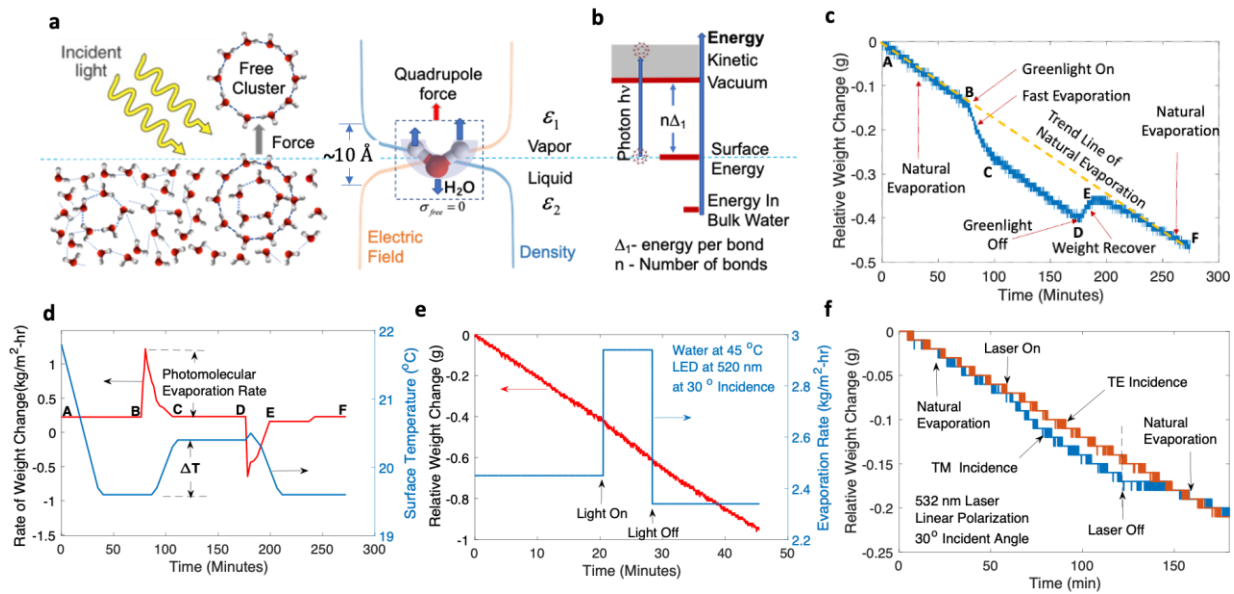


**Fig. 1 Photomolecular effect and evidence from weight change.** **a**, The physical picture of photomolecular evaporation: the perpendicular component of the electrical field of the incidence light changes by a factor of two over the distance of density change ( $\sim 10 \text{ \AA}$ ), creating a net force imbalance on water clusters existing at the interface that cleaves off the cluster. **b**, Energy conservation: the photon energy is used to break bonds of the water cluster with surrounding water molecules, the excess energy is converted into the cluster's kinetic energy. **c**, Weight loss as a function of time of pure water under green LED illumination with a nominal incident angle of  $30^\circ$  at ambient temperature  $22.2 \text{ }^\circ\text{C}$  and humidity 26%, AB-natural evaporation, B-LED is turned on, BC-rapid weight loss followed by slowing down, CD-steady state weight loss, D-LED is turned off, DE-weight recovery, EF-natural evaporation. **d**, Evaporation rate and surface temperature change with time corresponding to **c**. **e**, Weight loss when water is electrically heated to  $45 \text{ }^\circ\text{C}$  with the rest of conditions are similar to **c**, showing high photomolecular rate can be sustained under light. **f**, Weight loss when water is irradiated with polarized 532 nm laser light at  $30^\circ$  angle of incidence, showing that only TM polarization leads to the photomolecular effect.

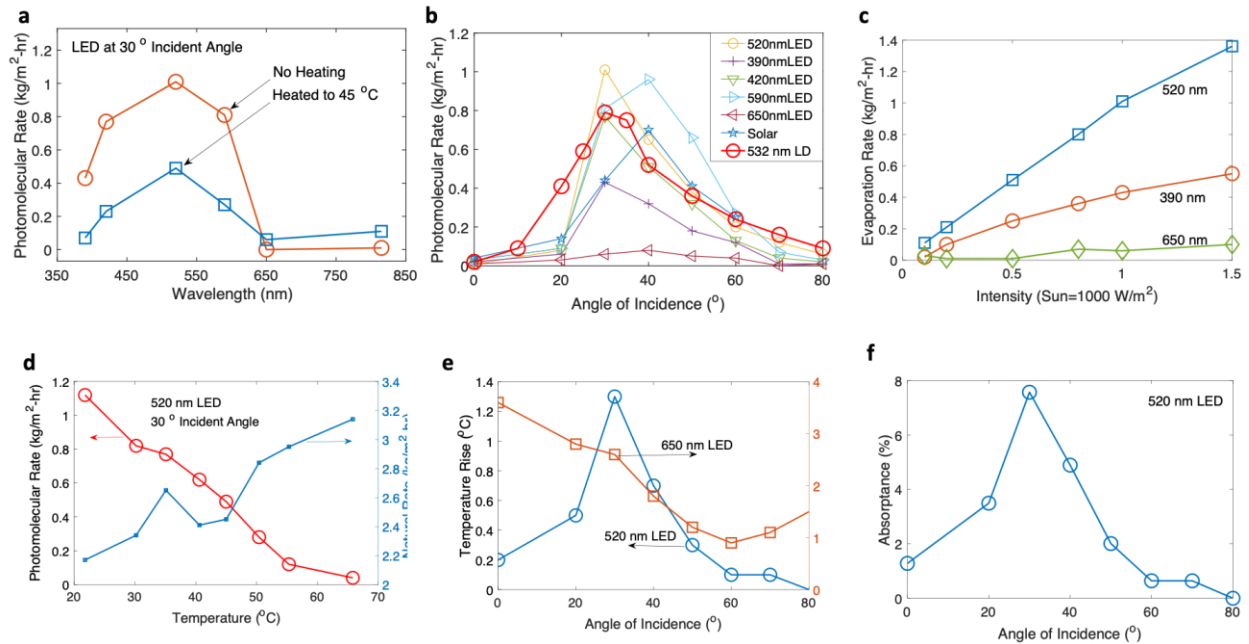


**Figure 2 Dependence of Photomolecular Evaporation Rate on Wavelength, Angle, and Temperature.** **a**, Wavelength dependence, showing that the photomolecular effect occurs only when the wavelength is shorter than 650 nm due to the energy conservation requirement. **b**, Photomolecular rate as a function of the angle of incidence. The peak happens because, at a small angle of incidence, the electrical field component of the incident light perpendicular to the surface is small, while at a large angle of incidence, the number of photons reaching the interface is small. **c**, The dependence on intensity is linear at low intensity and tends to be sublinear at a higher intensity. **d**, Water temperature dependence, showing the photomolecular effect weakens at a higher temperature because the cluster numbers in water are reduced. **e**, The temperature rise of water after the light is turned on, as a function of the angle of incidence, which is similar to the photomolecular evaporation rate in **b**. **f**, Calculated absorbance as a function of the angle of incidence.

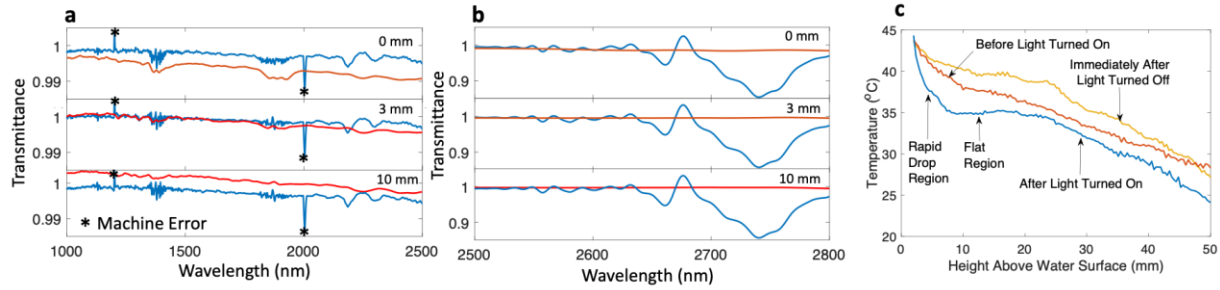


**Fig. 3 Signatures from the Vapor Phase under Green LED at 30° Incidence. a&b,** Comparison of the vapor transmission spectra at different heights between the light on (blue curves), and light off (red curves). When the light is on, fine lines appear. In the fundamental vibration wavelength around 2750 nm, the differences are large. **c,** Vertical vapor phase temperature distribution above water surface: the temperature drops more rapidly near the surface region when the light is turned on because clusters breaking off absorbs heat. The flat region happens because air is supersaturated with water vapor. When light is turned off, the temperature becomes higher because the cluster's condensation generates heat.

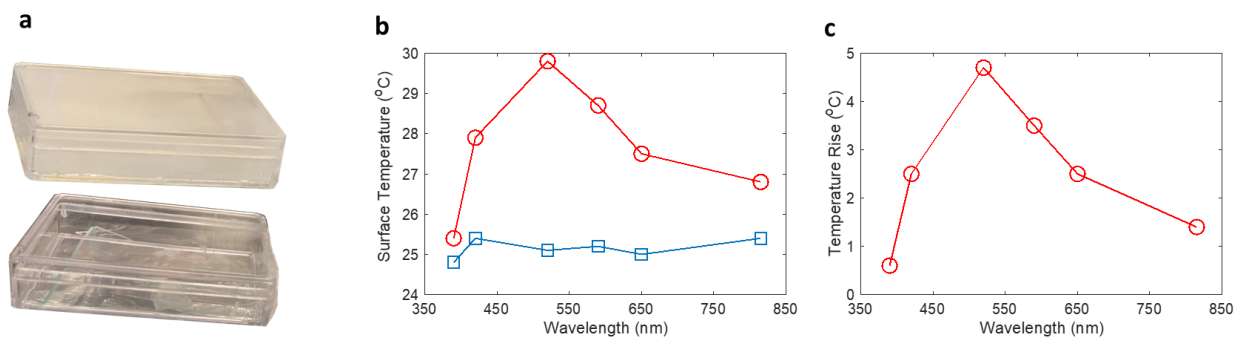
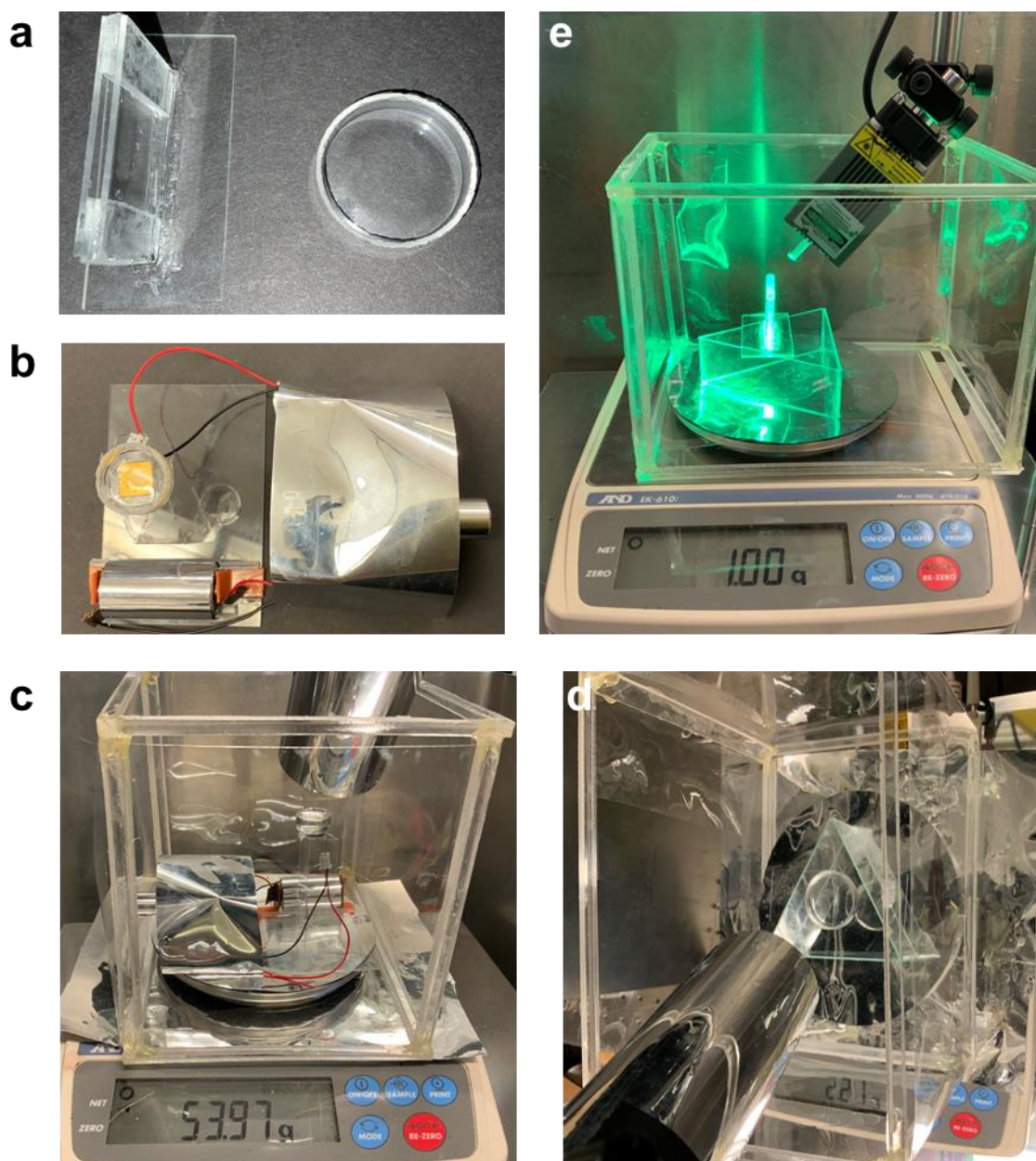
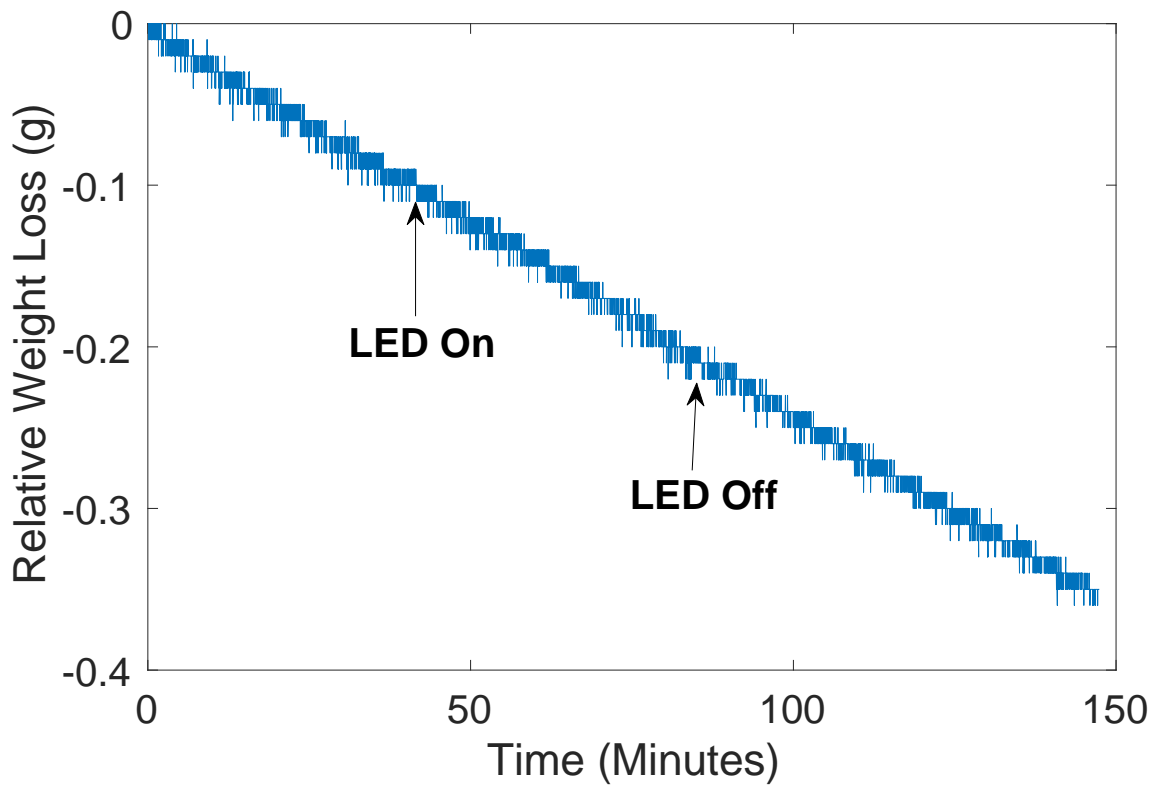


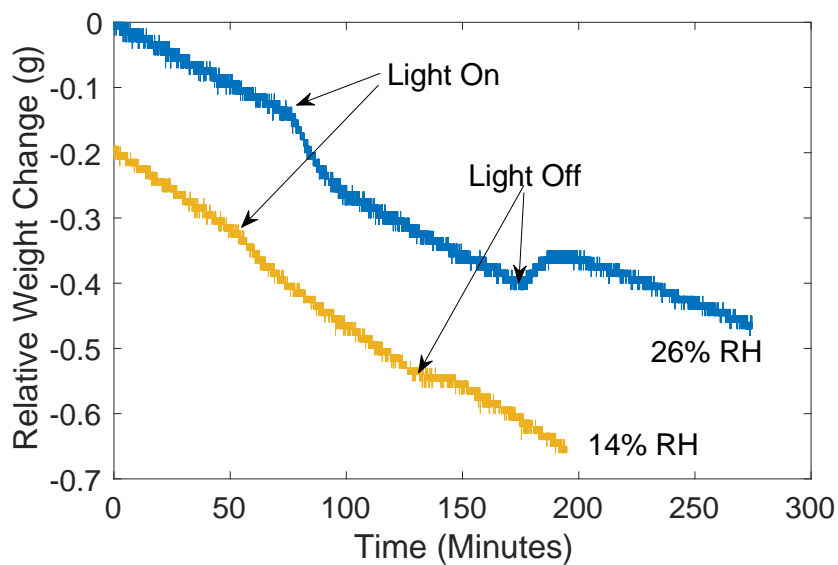
**Fig. 4 Heating of fog using green LED.** **a**, The photon of the fog chamber. **b**, The temperature rise of the clouds in a chamber under different LED illumination (1 Sun). The blue curve is the temperature rise of the empty fog holder, showing that the chamber itself does not absorb. **c**, Net temperature rise.



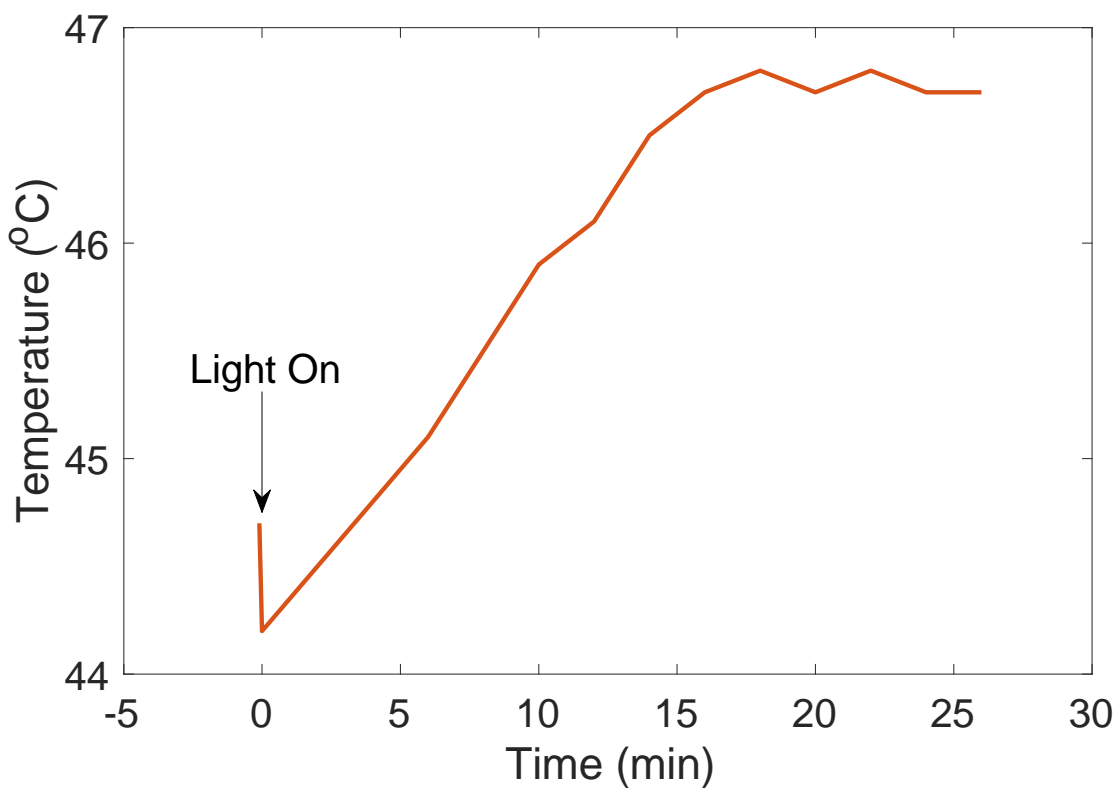
**Extended Data Fig. 1. Weight measurement platform.** **a**, Photos of containers: LED experiment uses circular glass water container with diameter 25 mm, water depth 3 mm. The laser diode experiment uses a rectangular water container, 2 mm wide and 18 mm in length, glued together from glass to make sure that the laser beam is larger than the surface area. If the light spot is too small compared to the free water surface area, natural evaporation will overwhelm the photomolecular signal. **b**, Joule heating setup: a heater is glued to the bottom of the container. The heater is driven by a battery and voltage controller by a potentiostat wrapped in a piece of aluminum foil. **c**, All Joule heating accessories are fitted on a weighing platform to minimize vibration noise to weight measurement. **d**, LED-driven evaporation, showing the water container is supported by nonabsorbing glass on weight platform, the windshield is made of plastic. **e**, The platform is under laser diode illumination.



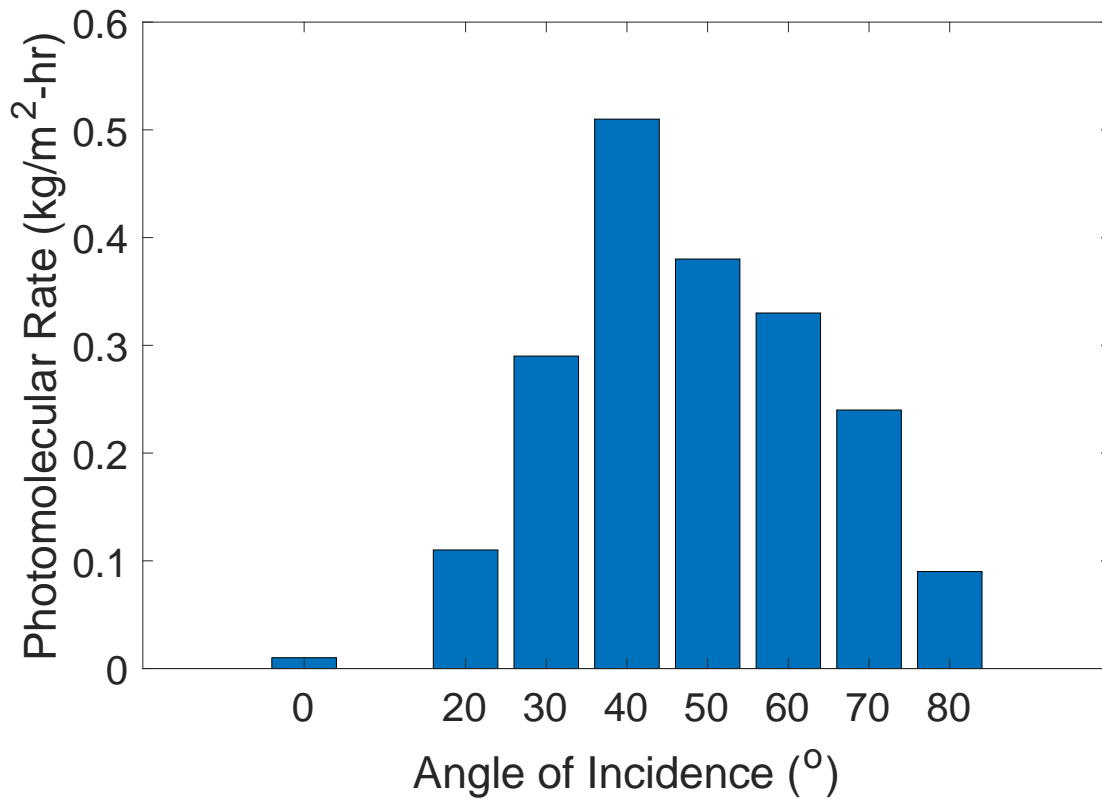
**Extended Data Fig.2. Weight history for LED at normal incidence.** When 520 nm LED is at the normal incidence, the water weight loss does not change when the LED is turned on and off, because in this case, there is no electrical field perpendicular to the interface and hence no quadrupole force acting on water clusters.



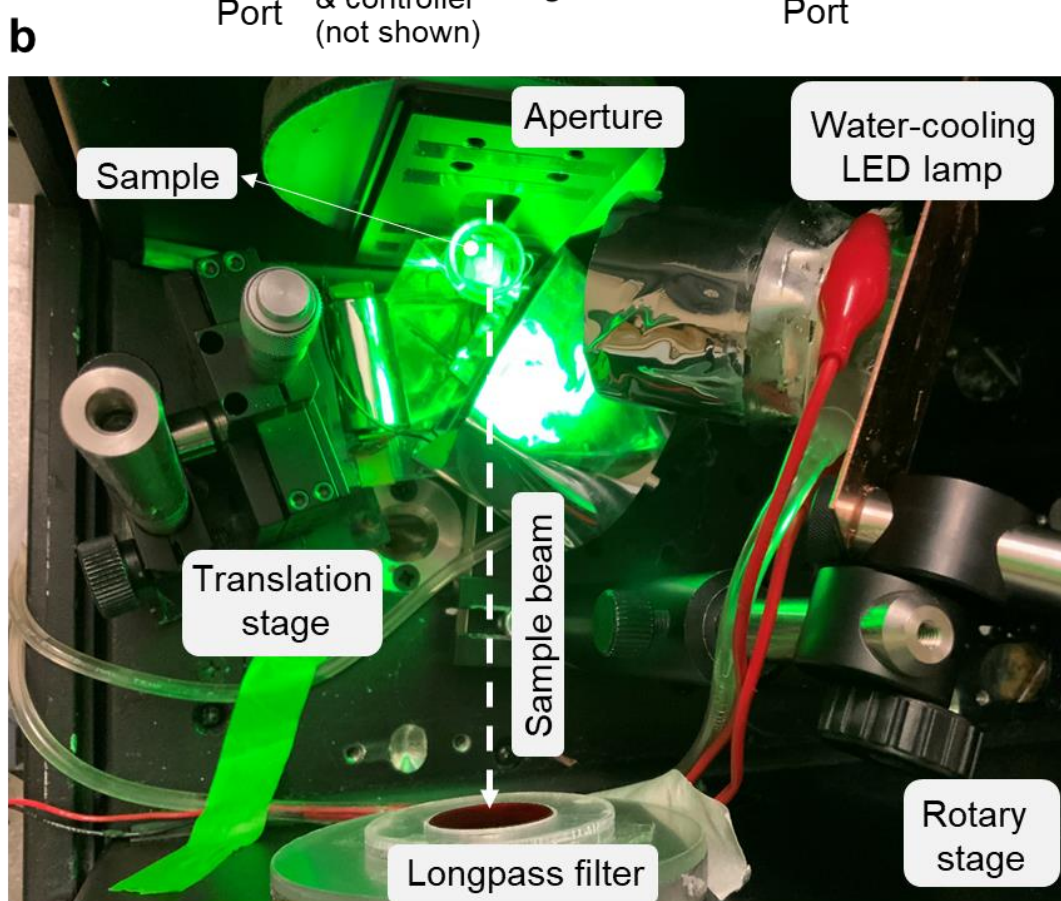
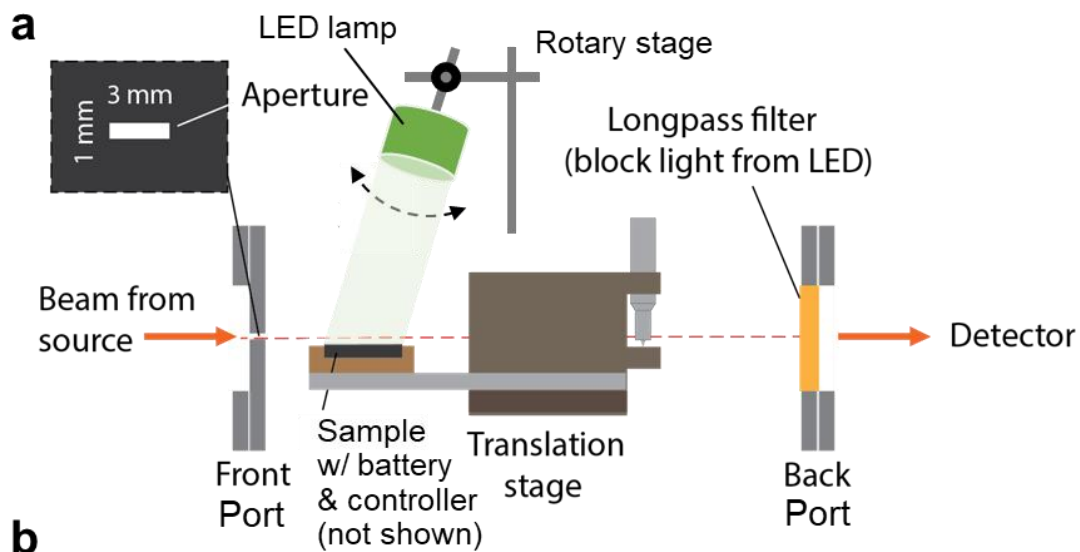
**Extended Data Fig.3. Humidity effect.** Different evaporation histories depend on humidity. At 26% humidity, the weight recovered when light (520 nm, 30° incidence) was turned off, i.e., the photomolecular levitation phenomenon. At 14% humidity, the weight did not recover after the light was turned off, although, for some time, the weight stays almost constant, i.e., the evaporation rate is lower than that of natural evaporation, because the recondensation balances the evaporation.



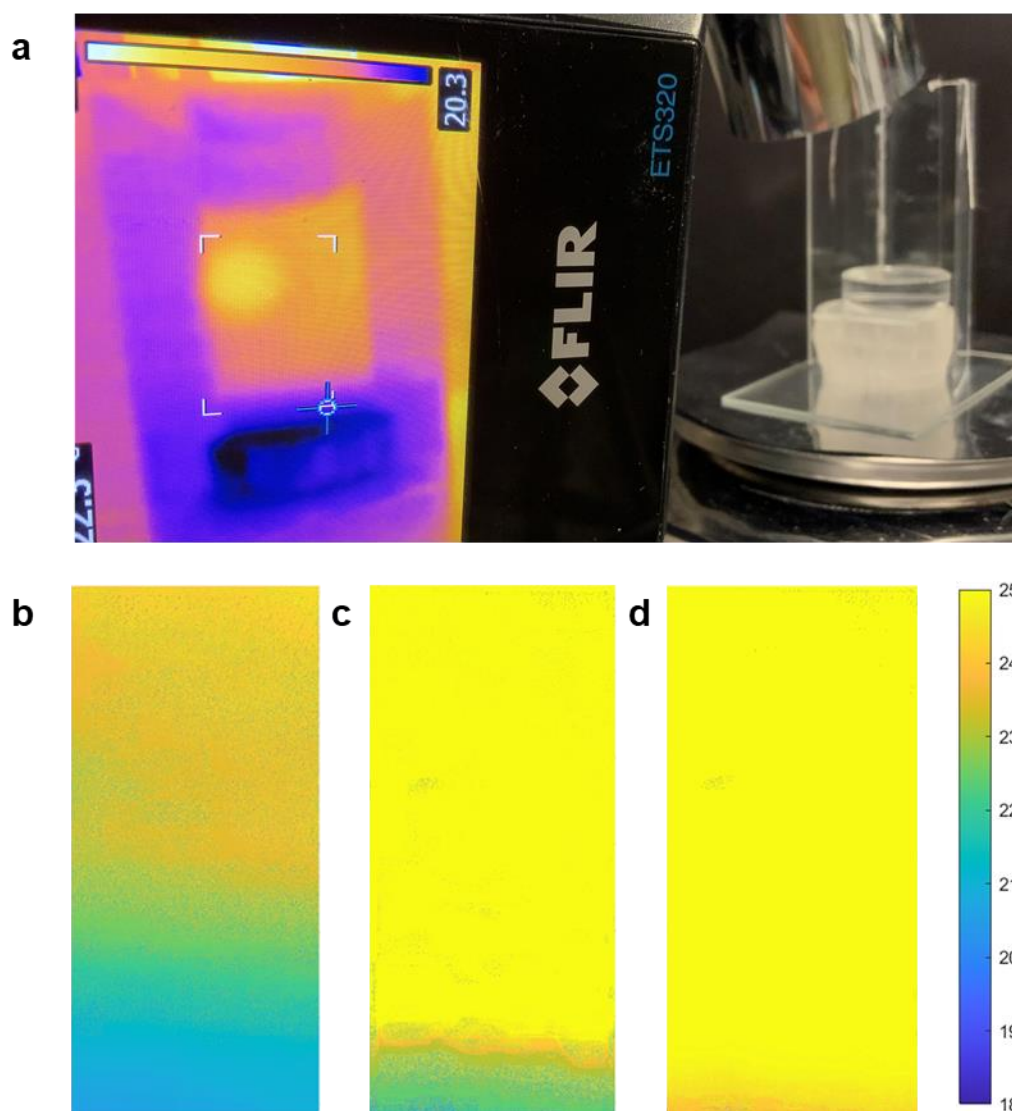
**Extended Data Fig.4. Surface temperature history when water was initially heated.** When the light is turned on (520 nm, 30° incidence), a small drop in surface temperature happens caused by the photomolecular evaporation, followed by temperature rise as some clusters condense while others are taken away by rising plumes.



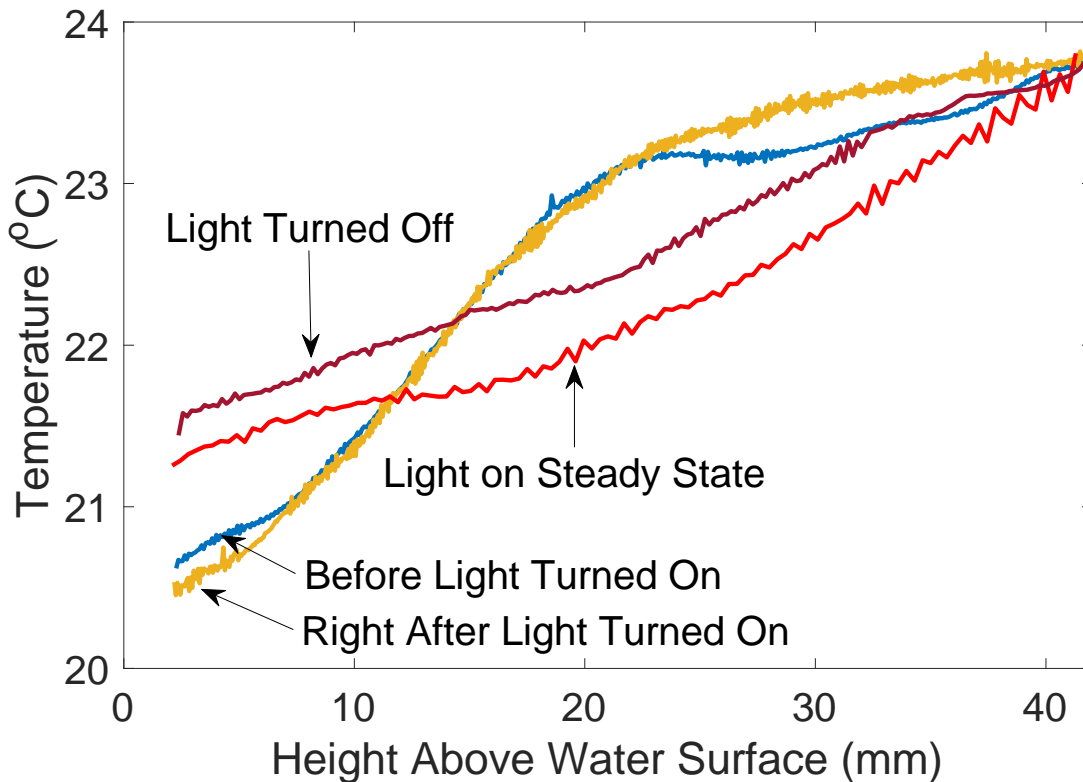
**Extended Data Fig.5. Angular dependence at high temperature.** Photomolecular rate measured when water is heated to 45 °C, using 520 nm LED, at a different angle of incidence. The evaporation rate has a peak at a 40° angle of incidence, similar to photomolecular evaporation at room temperature, although the rate is smaller.



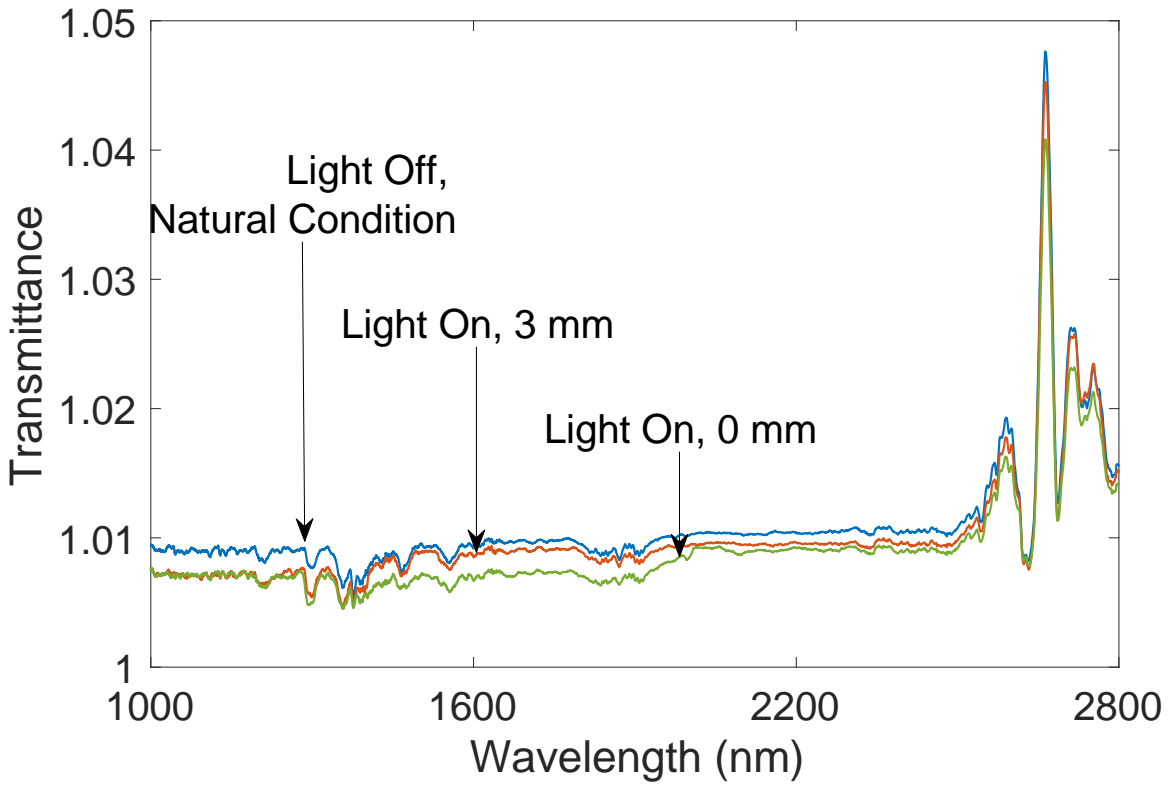
**Extended Data Fig.6. Vapor-phase UV-VIS transmittance set up.** (a) Illustration and (b) photo of a sample stage for vapor phase absorbance measurement inside a Cary 5000 UV-VIS-NIR spectrometer.



**Extended Data Fig.7. Vapor phase temperature distribution measurement.** **a**, The photo shows a glass slide hanging over the sample surface. The glass slide thermalizes with vapor and serves as an infrared emitter. **b-d**, IR images show the vapor temperature distribution over the pure water **b**, under dark conditions, **c**, right after green LED power-on (1 sun with 30° of incidence), and **d**, before green LED power-off (1 sun with 30° of incidence).



**Extended Data Fig. 8. Vapor phase temperature profiles.** The temperature profiles in the vapor phase at different times when water is not heated, obtained from average the IR image measured temperature distributions for 520 nm LED at a 30° of incidence. Right after the light is turned on, a small cooling happens because of photomolecular bond breaking, while at a steady-state, recondensation generates heat and raises the water surface and vapor temperature. When light is turned off, more heat is generated because of the condensation in supersaturated vapor.



**Extended Fig. 9. Vapor phase transmission when water is not electrically heated.** In this case, no appreciable difference can be observed because clusters are close to the surface.



**Extended Data Fig. 10. Fog experimental setup.** Fog generated by an ultrasonic vibrator is injected into a plastic container. The ultrasonic vibrator is cooled to avoid heating the fog.

**Movie 1. Fog heating under green LED.** To clearly show the fog inside the chamber, here we coat a thin layer of hydrogel on the inside surface of the chamber cover to avoid droplet-like condense.